ИНСТИТУТ ЯДЕРНОЙ ФИЗИКИ
им. Г.И. Будкера СО РАН

V.M. Aulchenko, S.E. Baru, A.E. Blinov, V.E. Blinov,
A.E. Bondar, A.D. Bukin, V.R. Groshev,
S.G. Klimenko, G.M. Kolachev, A.P. Onuchin,
V.S. Panin, I.Ya. Protopopov, A.G. Shamov,
V.A. Sidorov, Yu.I. Skovpen, A.N. Skrinsky,
V.A. Tayursky, V.I. Telnov, Yu.A. Tikhonov,
G.M. Tumaikin, A.E. Undrus,
A.I. Vorobiov, V.N. Zhilich

TAGGING SYSTEM FOR SCATTERED ELECTRONS IN TWO-PHOTON REACTIONS AT THE MD-1 DETECTOR

ИЯФ 94-12

НОВОСИБИРСК

Tagging System for Scattered Electrons
in TWO-Photon Reactions at the MD-1 Detector

A B S T R A C T

The Tagging System (TS) of the MD-1 detector at the VEPP-4 collider was used for studying of two-photon reactions. A transverse magnetic field enables one to detect scattered electrons and positrons even at zero scattering angles. The TS was calibrated with the events of the single bremsstrahlung and Bhabha scattering processes. The final examination was performed using the two-photon process $ee \to ee\mu\mu$. The TS energy resolution for scattered electron was $\sigma(E)/E=1.75\%$ at the beam energy $E_0=4.7$ GeV. In the double-tag mode the resolution for a resonance with a mass of 3 GeV/c^2 was $\sigma(M_{inv})=0.12$ GeV/c^2 and the efficiency of tagging was about 10%.

1. Introduction

In this paper the results of long term operation of the Tagging System (TS) for detection of scattered electrons[1] in two-photon processes at the VEPP-4 collider are summarized. The main feature of the detector MD-1 is the magnetic field transverse to the orbit plane. This allows one to detect scattered electrons even with zero emission angles.

Some of the detectors (DM1, PLUTO, TASSO, CELLO, PEP-9, etc.) had specialized tagging systems for scattered electrons [1-5]. However, typical "taggers" covered the angular range between 20 and 100 mrad (except DM1) that resulted in the reduction of the efficiency and systematic errors caused by the dependence of amplitudes of the processes on the Q^2 value of the virtual photon.

[1)] Reference to a scattered electron implies a scattered positron as well.

Due to the good energy resolution and high detection efficiency for scattered electrons the information from the TS was used for double-tagged events as well as for single-tagged events. For double-tagged events M_{inv} of the produced $\gamma\gamma$-system can be determined with the accuracy 110÷200 MeV/c^2 using the TS information only. For single-tagged events the scattered electron parameters were used for kinematic reconstruction in the central part. For example, for the study of the $e^+e^- \to e^+e^-\eta \to e^+e^-\gamma\gamma$ process in a single-tag mode the invariant mass of $\gamma\gamma$-system was calculated without photon energy measurement.

The MD-1 detector was in operation at the VEPP-4 collider in 1980÷1985. The total integrated luminosity with the installed TS was 25 pb^{-1} in the mass region $\sqrt{s}$=7.6÷10.4 GeV. For the TS calibration the events of the single bremsstrahlung and Bhabha scattering processes were used. The events of the $e^+e^- \to e^+e^-\mu^+\mu^-$ process were used for the final check of the TS efficiency and energy resolution. Single-tagging was used for the measurement of the two-photon widths of η, η' and a_2 mesons [6] and double-tagging - for the measurement of the total cross section of the process $\gamma\gamma \to$hadrons [7].

2. Detector MD-1

The layout of the Magnetic Detector (MD-1) is shown in Fig. 1. The description of the detector and experiment can be found elsewhere [6,8-10]. Here we describe detector parameters relevant to the present analysis only.

The magnetic field in the detector is transverse to the orbit plane and equals 11.3 kG at the beam energy of 4.7 GeV. In the central part of the detector proportional chambers yield a momentum measurement with the resolution $\sigma_p/p=0.1 \cdot p$ (GeV/c) within a solid angle of $0.6 \cdot 4\pi$

Scintillation counters surround the coordinate system and cover a solid angle of $0.9 \cdot 4\pi$ The time resolution is 0.8 ns. Due to the presence of 1.7 radiation length (X_0) of material in front of the counters (the walls of the coordinate chamber volume) they provide good electron identification by the pulse height of the signal.

The system of shower-range chambers (SRC) consists of 14 separate units covering the solid angle of $0.8 \cdot 4\pi$. Each unit contains 10 layers of proportional chambers alternating with $0.74 \cdot X_0$ thick stainless steel plates. The pulse height of the signal from each chamber is used for the energy loss measurement.

The luminosity was measured using elastic Bhabha scattering at small angles. The monitoring system is placed

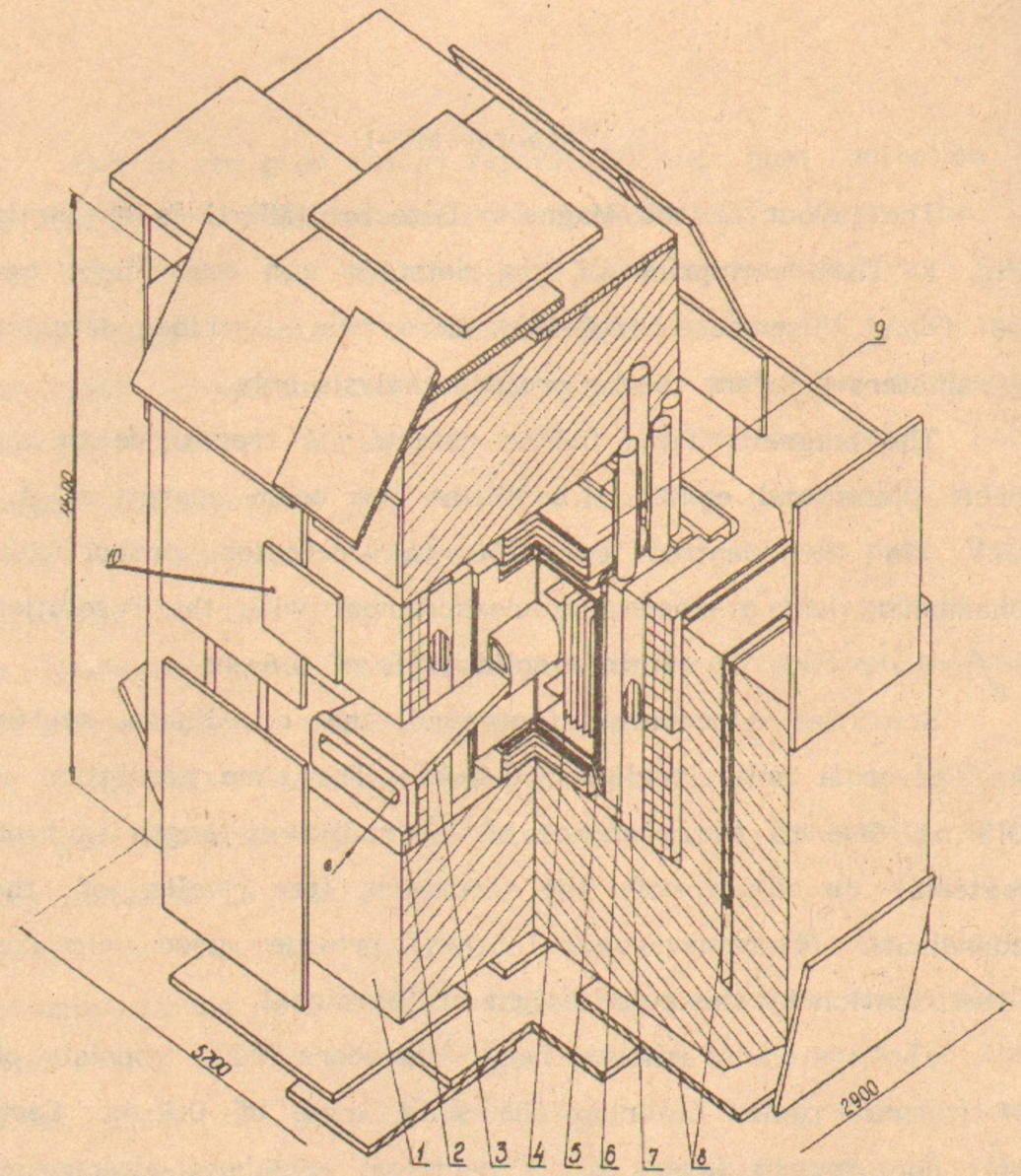

Fig. 1. Layout of the MD-1 detector.

directly behind the TS (Fig. 2 and 3). The absolute calibration of the monitor has been done by three independent methods: double bremsstrahlung in a special run [11], large angle Bhabha scattering [11] and process $ee \to \mu^+\mu^-$ [12]. The accuracy of the luminosity measurement was 2.2%.

Two NaI(Tl) crystals at zero angles detected photons of the single bremsstrahlung process. This information was used for the quick luminosity measurement and for the suppression of the background in the TS. There was a lead shield of 18 mm thickness placed in front of the NaI detector for protection against the synchrotron radiation.

3. Tagging system

Two-photon processes at e^+e^- colliders are studied in the reactions $ee \to ee\gamma^*\gamma^* \to eeX$, where γ^* is a virtual photon. Detection of the scattered e^+e^- in the final state allows one to determine parameters of the produced system X. The transverse field of the MD-1 detector deflects the scattered electron from the beam and directs them to the TS, which is placed 3.5 m downstream from the interaction point at the distance of 5 cm from the beam. The TS volumes are separated from the vacuum chamber by a thin foil. To keep the synchrotron radiation background at an acceptable level

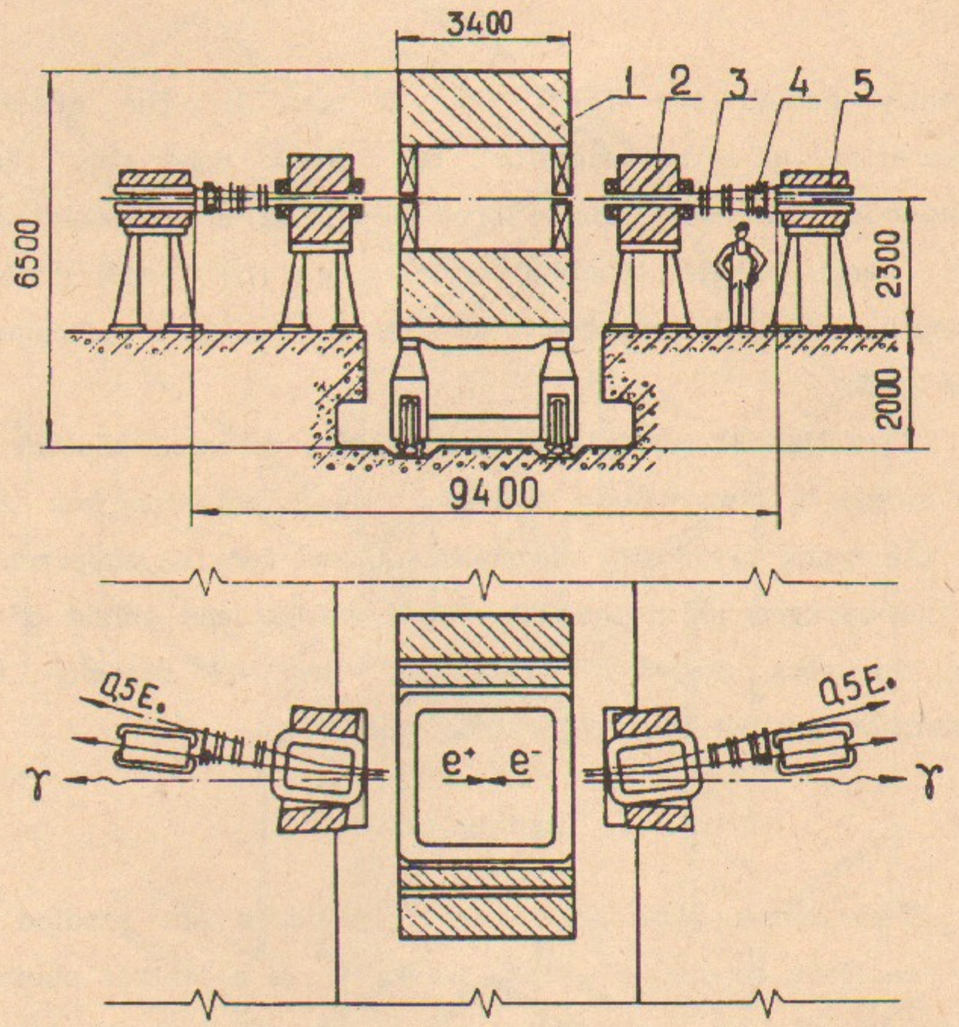

Fig. 2. Layout of the interaction region.
1- MD-1 detector, 2-bending magnets, 3, 4- Tagging systems and luminosity monitor, 5-lenses.

additional absorbers were used. The total thickness of material in front of TS was $0.06 \cdot X_0$. From both sides of the detector additional 7 kG magnets were installed to improve the TS energy resolution and increase TS acceptance. The layout of the MD-1 detector with the TS is shown in Fig. 2.

Scattered electrons were detected in the energy range of $(0.50 \div 0.85) \cdot E_0$ even at zero scattering angle, where E_0 is the beam energy. Electrons with other energies are detected due to nonzero scattering angle. For the energy E_0 the electrons were detected in the range $\pm(14 \div 25)$ mrad in the vertical direction and $-14 \div +75$ mrad in the orbit plane.

The TS consists of two blocks. Each block contains 7 proportional chambers. Three chambers measure a vertical (Z) coordinate, other three measure a radial coordinate (Y) and the seventh one determines a coordinate inclined at the angle of 45° to the orbit plane (T), that is necessary for pattern recognition. Y- and Z-chambers have a C-like shape and envelope the beam pipe from three sides. The sensitive radial size of the chambers is 500 mm, the vertical - 200 mm. Behind TS there is the system of four scintillation counters for luminosity measurement and a sandwich $(5 \cdot X_0)$ used both for luminosity measurements and triggering. The layout of the chambers inside the TS block is shown in Fig. 3. For Z- and T-coordinate measurements the ordinary

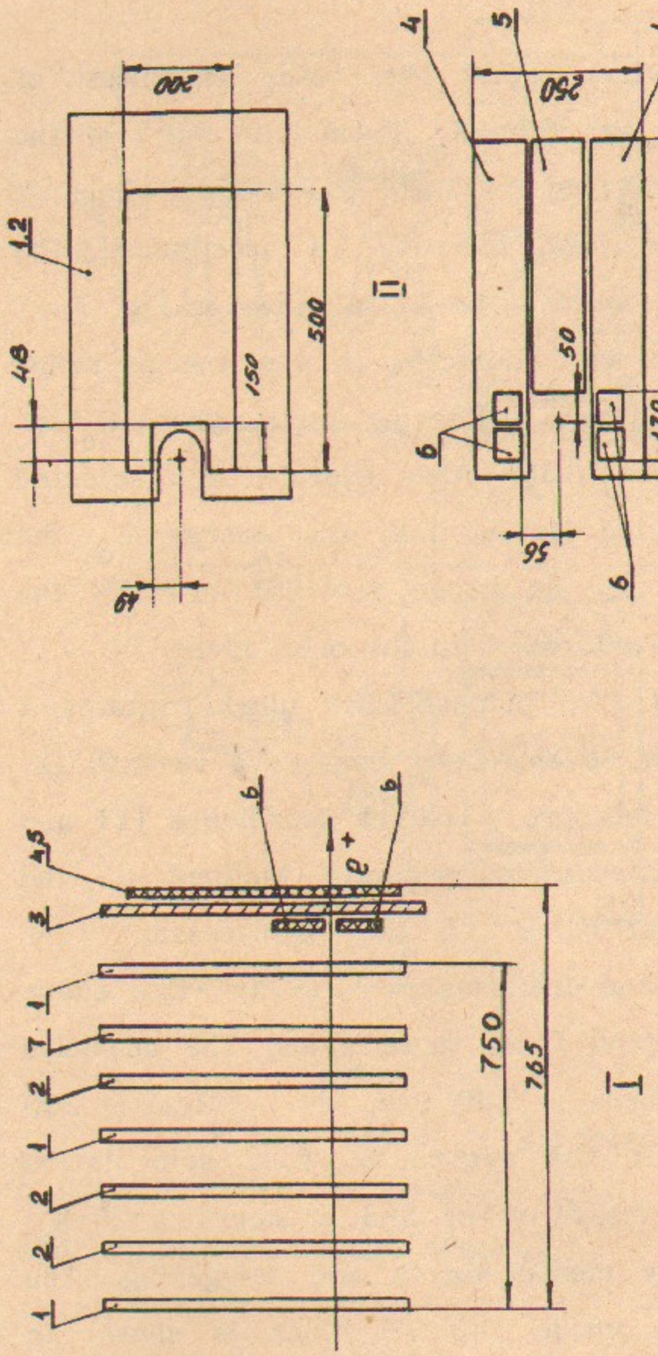

Fig.3. Tagging system for scattered electrons. II- beam view of the chambers, III- beam view of the counter. 1 - Y-chambers for radial coordinate, 2 - Z-chambers for vertical coordinate, 3 - $5 \cdot X_0$ W converter, 4,5 - scintillation counters of the TS, 6 - scintillation counters for luminosity monitoring, 7 - T-chamber.

proportional chambers are used. The step of the anode wires is 4 mm for Z- and 3 mm for T-chambers. For the Y-coordinate measurements the induction chambers with cathode delay line (DL) read-out were chosen [13-15]. The Y-chamber cathode plane was divided into 5 parts to provide uniform distribution of the counting rate. The orbit plane (Z=0) crosses three of them. Each part was coupled to its own DL. The time difference of the pulse arrival to the DL ends contains the information about the particle coordinate along the anode wire.

This system provides the resolution $\sigma_z \sim 1$ mm, and $\sigma_y \sim 0.25$ mm at small counting rates (σ is defined as FWHM/2.36). More detailed description of the TS, chambers and electronics can be found in ref. [16,17].

4. Calibration of the TS

The measurement of coordinates and angles of the electron in the detection system allows one to determine the relative energy $\nu = E_e / E_0$ and emission angles ϑ_y and ϑ_z when the position of the interaction point is known. The location of the interaction area was determined by the vertex reconstruction for multihadron events in the central part of the detector. The slow drift was observed and taken into

account. For the whole period of the experiment it was 3 mm for Y and 1 mm for Z.

The energy resolution is determined mainly by the accuracy of the angle measurement in the orbit plane. Multiple scattering in the entrance foil contributes σ_E/E_e=1.5% at E_0=4.7 GeV (proportional to $1/E_0$) and the spatial resolution of the Y-chambers - $3.7\cdot\nu\cdot\sigma_Y$ [mm]%. The size of the interacting area is 35×0.7×0.02 mm^3 and its influence on the energy resolution is small in our case (less than 0.3%).

The angular resolution in the orbit plane $\sigma(\vartheta_Y)$ is determined by the same factors as σ_E as wells as by the size of interaction area along the orbit. The mean value of $\sigma(\vartheta_Y)$ is 2.5 mrad. The $\sigma(\vartheta_Z)$ resolution (along magnetic field) determined by the spatial resolution of Z-chambers and the beam angular spread is about 0.3 mrad.

In separate tests the spatial resolution of the Y-chambers σ_Y~0.15 mm was obtained in cases of small irradiated areas. But under the real experimental conditions the σ_Y resolution for the whole area of the chamber was considerably worse. It is explained by some systematic errors of the time-coordinate calibration procedure, which was performed with the generator signals fed into the certain points of the cathode plane. Besides that there is

huge nonlinearity near the DL ends.

To correct these systematic errors the information from T-chamber was used. For the single bremsstrahlung process there is an unambiguous dependence of the coordinate in Y-chambers and in the T-chamber because of the small emission angle of electrons. The T-coordinate is determined by the number of the fired wire with known position. In Fig.4a the difference between the Y-coordinates measured by Y- and T- chambers is shown. There are considerable deviations near the DL-ends and relative shifts.

To eliminate these deviations the empirical formula with 6 parameters was fitted for every DL. The results of the corrections are shown in Fig. 4b. To exclude the influence of the long term electronic instability this procedure was performed for the whole experiment with a step of 1 month.

After corrections the spatial resolution on Y for the whole area of the chambers was 0.27 mm for the runs with a low luminosity (counting rate is less than 10 kHz per chamber) and became 0.33 mm for the typical experimental conditions (luminosity $L=3\cdot10^{30}cm^{-2}\cdot sec^{-1}$, counting rate up to 400 kHz per chamber). The main causes of the spatial resolution change for the worse in the experiment are the following: the remaining differential nonlinearity of the

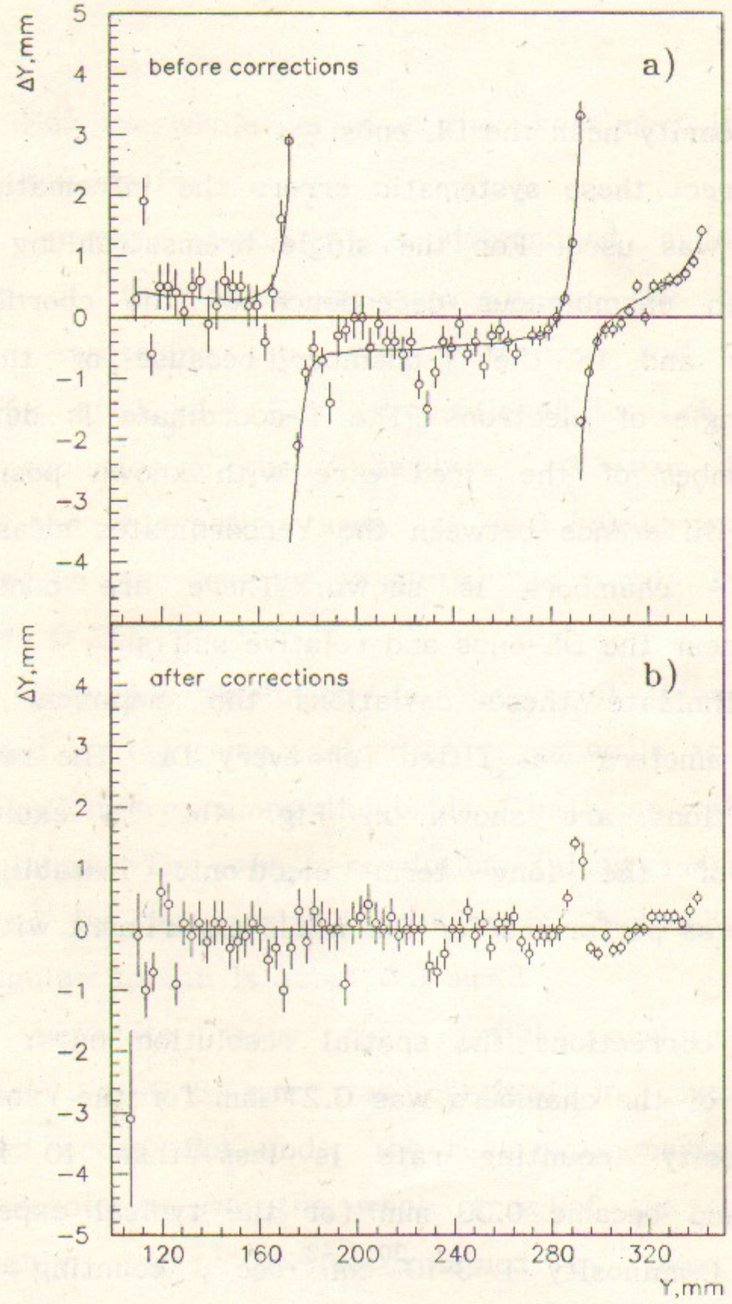

Fig.4. Deviation of the measured Y-coordinate from the calculated one. a) Before corrections. b) After corrections.

Y-chambers, firstly; two or more particles hitting the one DL, secondly (the overlap probability is about 10% for $L=3\cdot10^{30}cm^{-2}\cdot sec^{-1}$). The dependence $\sigma_y(L)$ is shown in Fig. 5. With increasing of L, the FWHM grows slowly, but the true sigma (R.M.S) increases faster because of the long "tails" caused by extra particles.

In the case of the high rate some loss of Y-chamber efficiencies was observed. At $L=3\cdot10^{30}cm^{-2}\cdot sec^{-1}$ the inefficiency reaches 20%. There are two reasons: the space charge, which causes the decrease of the signal pulse height; and overlapping with extra particles. Dependence of the inefficiencies of single Y- and Z-chambers on the luminosity are shown in Fig. 6. The efficiency of Z-chamber is stable, but for Y it falls down with luminosity growing. In spite of these problems the efficiency for straight trajectory reconstruction in the TS was 97%. The efficiency decrease due to wire aging during the whole experiment was less than 5% for the chambers with maximum counting rate.

For the energy calibration of the TS special runs at low luminosity were performed [11]. The events of single bremsstrahlung processes were used. The γ-quantum energy was measured by the total absorption NaI(Tl) counter, which was calibrated by the edge of the bremsstrahlung photon spectrum. This calibration allowed us to obtain necessary

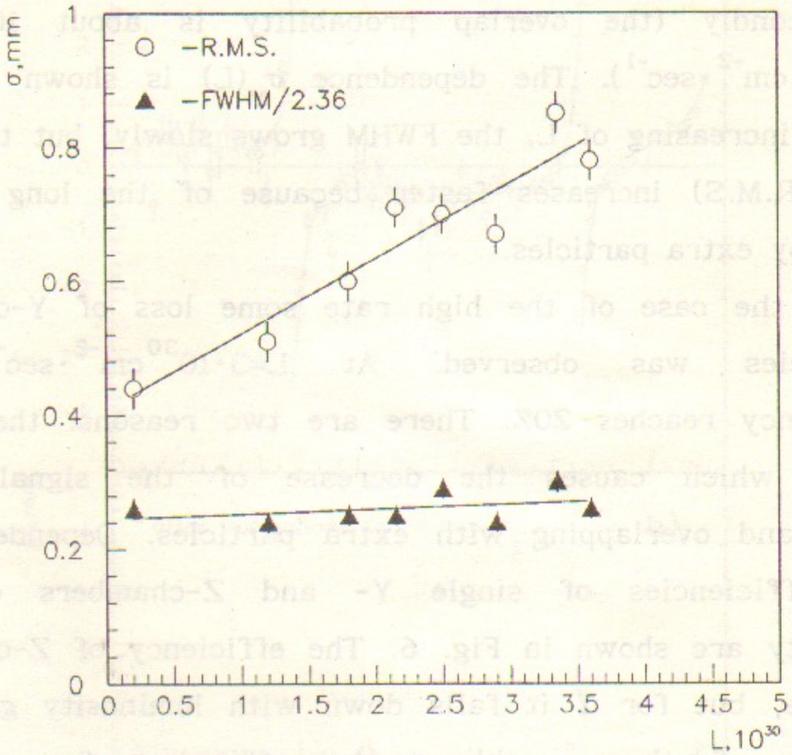

Fig.5. Dependence of the spatial resolution of the Y-chamber on the luminosity.

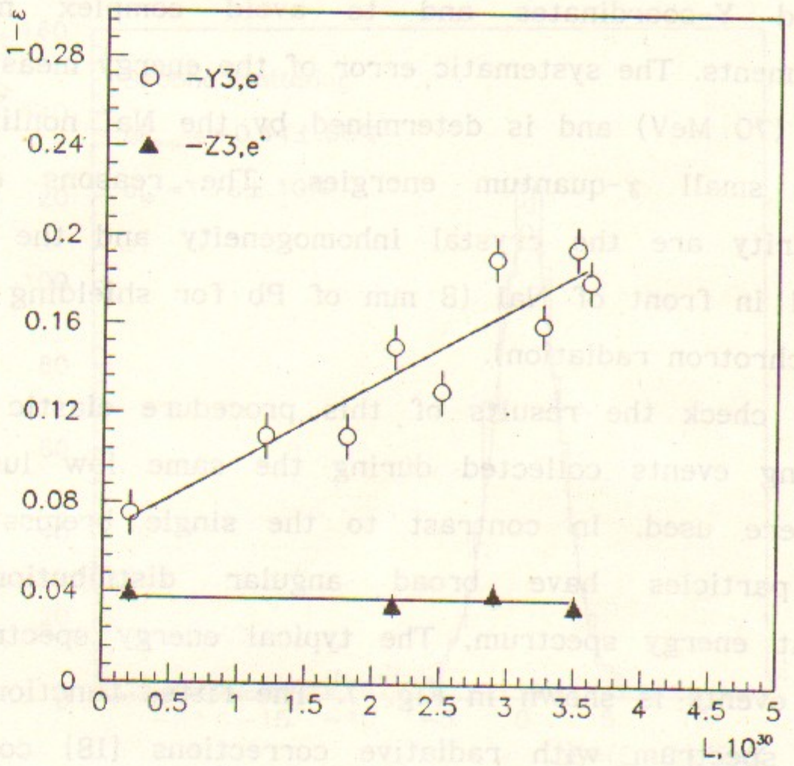

Fig.6. Dependence of the inefficiency of the most irradiated chambers on the luminosity.

coefficients connecting the electron energy with the measured Y-coordinates and to avoid complex magnetic measurements. The systematic error of the energy measurement is 1.5% (70 MeV) and is determined by the NaI nonlinearity at the small γ-quantum energies. The reasons of this nonlinearity are the crystal inhomogeneity and the passive material in front of NaI (8 mm of Pb for shielding against the synchrotron radiation).

To check the results of this procedure elastic Bhabha scattering events collected during the same low luminosity runs were used. In contrast to the single bremsstrahlung these particles have broad angular distributions and different energy spectrum. The typical energy spectrum for Bhabha events is shown in Fig. 7. The fitted function is the Bhabha spectrum with radiative corrections [18] convoluted with the sum of two Gaussians. The width (σ_{bh}=FWHM/2.36) and the peak position are in agreement with our expectations. The dependence of the measured σ_{bh} on $1/E_0$ is shown in Fig.8. It agrees with calculations, the growth is explained by multiple scattering in the entrance foil and absorber. The lower line is the contribution of the Y-chamber spatial resolution. For the E_0=4.7 GeV the energy resolution is $\sigma_{bh}/E_0=(1.7\pm0.1)\%$. The energy shift is less than 2%.

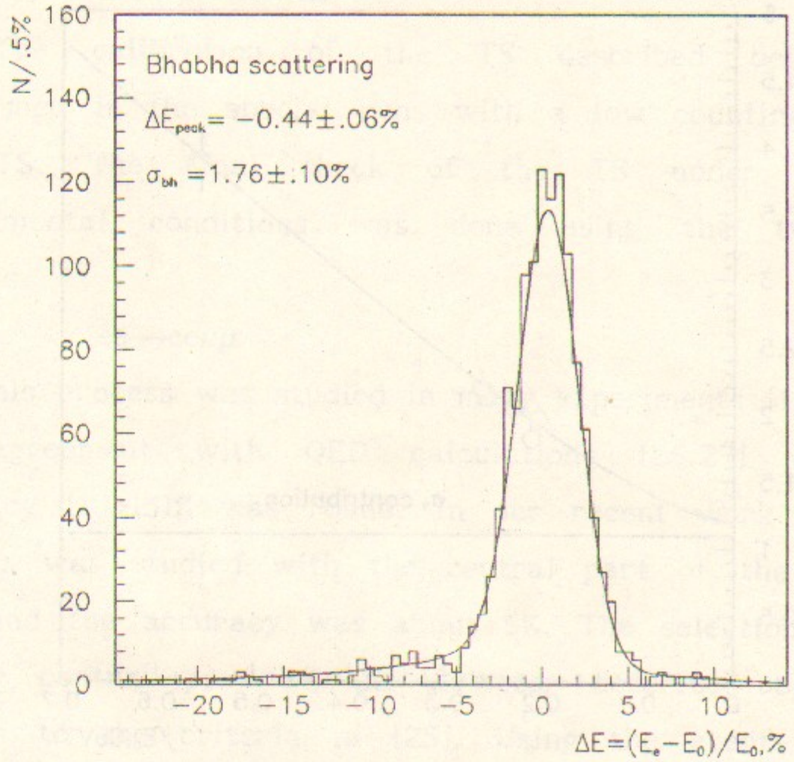

Fig.7. Energy spectrum for Bhabha scattered electrons detected in the TS.

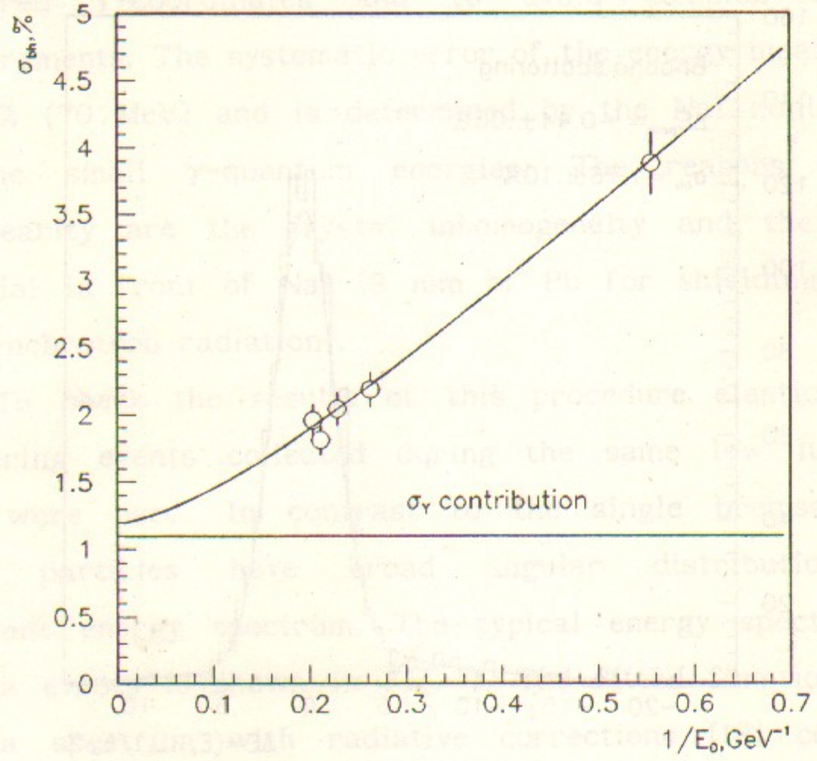

Fig.8. Dependence of the energy resolution σ_E/E for Bhabha scattered events on the beam energy E_0. Upper line - MC simulation, lower line - contribution of the spatial resolution of Y-chambers.

5. Selection of the $ee \to ee\mu\mu$ events

The calibration of the TS described before was performed in the special runs with a low counting rate in the TS. The final check of the TS under the real experimental conditions was done using the two-photon process

$$ee \to ee\mu\mu. \qquad (1)$$

This process was studied in many experiments [19-24] and the agreement with QED calculations [26,27] with the accuracy (10÷15)% was found. In our recent work [25] this process was studied with the central part of the detector only and the accuracy was about 5%. The selection criteria in the central part of the detector described below are similar to the criteria in [25]. Using the events selected with the central part information only (no-tag) we can check the TS for the absolute efficiency and energy calibration in single- and double-tag modes.

The total cross section for the process (1) is 61.8±0.2 nb at E_0=4.73 GeV. The main physical background comes from the two-photon reactions

$$ee \to eee^+e^- \qquad (2)$$

$$ee \to ee\pi^+\pi^-. \qquad (3)$$

The cross section of the process (2) is by a factor 10^5

larger than that of (1), but most of the ee-pairs are strongly boosted and escape the detector. The visible cross sections of the reactions (1) and (2) are of the same order.

The events with two opposite-charged particles were selected with the momenta 250<R<2500 MeV/c, acomplanarity angle $\Delta\varphi<20^0$. The acolinearity angle $\Delta\omega>10^0$ was required to reduce the background from cosmic rays and the two particle reactions $ee\to e^+e^-(\mu^+\mu^-)$. To suppress the background of multihadron events the number of triggered scintillation counters was required to be 1÷3 and the number of shower-range units - 1÷2. Additional cosmic ray rejection was performed using the time-of-flight information from scintillation counters.

After that in the region $M_{inv}(\mu^+\mu^-)=0.35\div2.0$ GeV/c^2 (considering all particles as muons) the fraction of $\gamma\gamma\to\mu^+\mu^-$ was about 50%. Other events came from $ee\to e^+e^-$, $\gamma\gamma\to e^+e^-$, $\gamma\gamma\to\pi^+\pi^-$ and beam-gas interactions. Additional suppression of the background from $ee\to e^+e^-$ and $\gamma\gamma\to e^+e^-$ was done using the pulse height information from the shower-range chambers and scintillation counters. After all cuts we obtained about $12\cdot10^3$ events for the integrated luminosity 23.6 pb^{-1}, mainly from reactions (1) and (3).

The Monte-Carlo (MC) simulation of the $ee\to ee\mu\mu$ process was done using the Berends generator [28] where the

radiative corrections are taken into account. The accuracy of the algorithm is about 0.3%. The detector response was simulated by the UNIMOD code [29]. The measured efficiencies of the detector components and signal-background coincidences, which caused the loss of the true events, were taken into account. After imposing the described cuts 7955 events for the generated 17.9 pb^{-1} were selected. The statistical error for σ_{vis} is 1.1% while the systematic one is 3.0%. The systematic error arises mainly from the inefficiency of the coordinate chambers of the detector and the background corrections.

The contribution of the $\gamma\gamma\to\pi^+\pi^-$ process was found to be (20±3)% using the MC simulation (Born term interfering with $f_2(1270)$ meson). The error is determined by the uncertainty in the $\gamma\gamma\to\pi^+\pi^-$ cross section.

The mass difference between $\mu^\pm$ and $\pi^\pm$ (even with $e^\pm$ at $M_{inv}>1$ GeV/c^2) gives small effect on calculated parameters of the scattered electrons (see section 6). Therefore reaction (1)-(3) were used in our analysis ((2) gives only a 4% contribution).

The contribution of other background processes in our final sample was estimated using the real experimental data and MC simulation. In Table 1 their values are listed.

Table 1. The results on selection of the process $ee \to ee\mu\mu$.

		experiment	MC
Integrated luminosity, pb^{-1}		23.6 (±2.2%)	17.9 (±0.3%)
Number of selected events, N_0		12334	7955
Background contributions,		N_b/N_0	
Background	Method of estimation		
$\gamma\gamma \longrightarrow \pi\pi$	(MC)	20.±3.0%	-
$\gamma\gamma \longrightarrow ee$	(MC)	3.8±1.2%	-
$\gamma\gamma \longrightarrow KK,\tau\tau$	(MC)	0.5±0.1%	-
$ee \longrightarrow ee,\mu\mu$	(MC)	0.5±0.4%	-
cosmic rays	(exp)	0.5±0.2%	-
$ee \longrightarrow$ hadr	(exp)	0.5±0.3%	-
beam-gas	(exp)	2.5±1.0%	-
$\sigma_{vis}(ee \longrightarrow ee\mu\mu)$, nb		0.452	0.444
Error of σ_{vis}, stat. and syst., %		±1.0±4.4	±1.1±3.0
$R=\sigma^{exp}_{vis}/\sigma^{MC}_{vis}$		1.018±0.010±0.054	

The results of the $ee \to ee\mu\mu$ cross section measurements are shown in Table 1. The measured cross section for $ee \to ee\mu^+\mu^-$ agrees with the QED calculations with the accuracy 5.5%. The systematic error of σ_{vis} for the experiment is mainly determined by the background

subtraction procedure, that for the MC - by inefficiencies of the detectors elements. The statistical error of the MC simulation is included into the systematic error of R.

The invariant mass distribution for the selected pairs is shown in Fig. 9. To all particles the muon masses were ascribed. The shape of the spectrum agrees with the MC one (sum of $\mu\mu$, $\pi\pi$ and ee) within 5% errors. The distributions over the transverse momentum P_t of the pairs and acomplanarity angle $\Delta\varphi$ Fig. 10 and 11) are also in reasonable agreement with the expectations.

So we have a sample of $\gamma\gamma$ events clean enough to be used for the check of the TS.

6. The $ee \to ee\mu\mu$ events with tagging of scattered electrons

To study the two-photon processes with the detection of one or two scattered electrons (single- and double-tag modes) it is necessary to know the accuracy of energy measurement and the efficiency of the TS under the real background conditions.

Using the measured momenta of the muons one can calculate the energies of both scattered electrons assuming that one of the scattered electrons (undetected one - for single-tag mode) has $P_t=0$. In Fig. 12(a) the spectrum on the

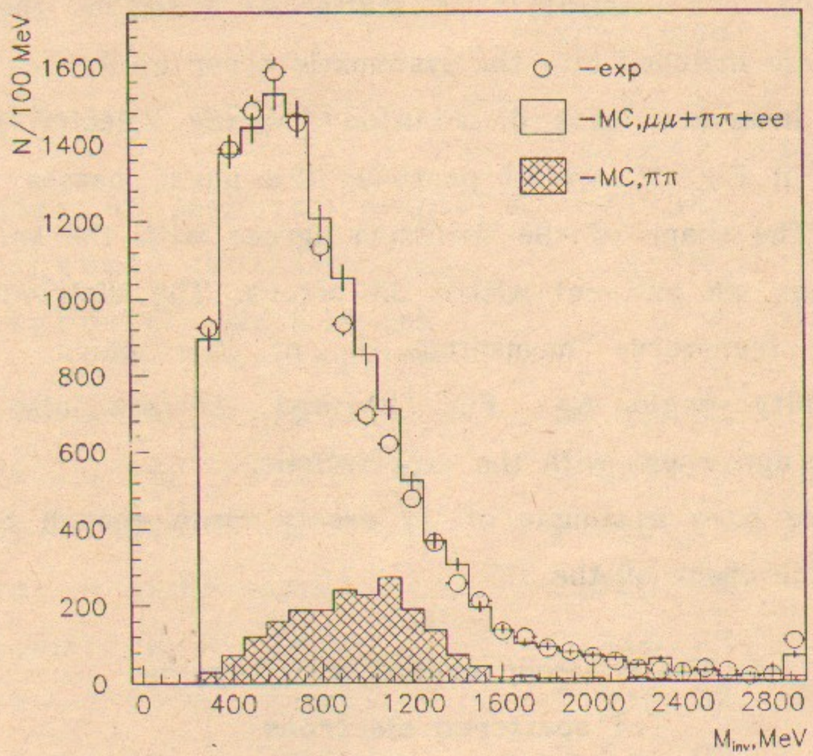

Fig.9. Invariant mass spectrum of selected pairs, all particles considered as muons.

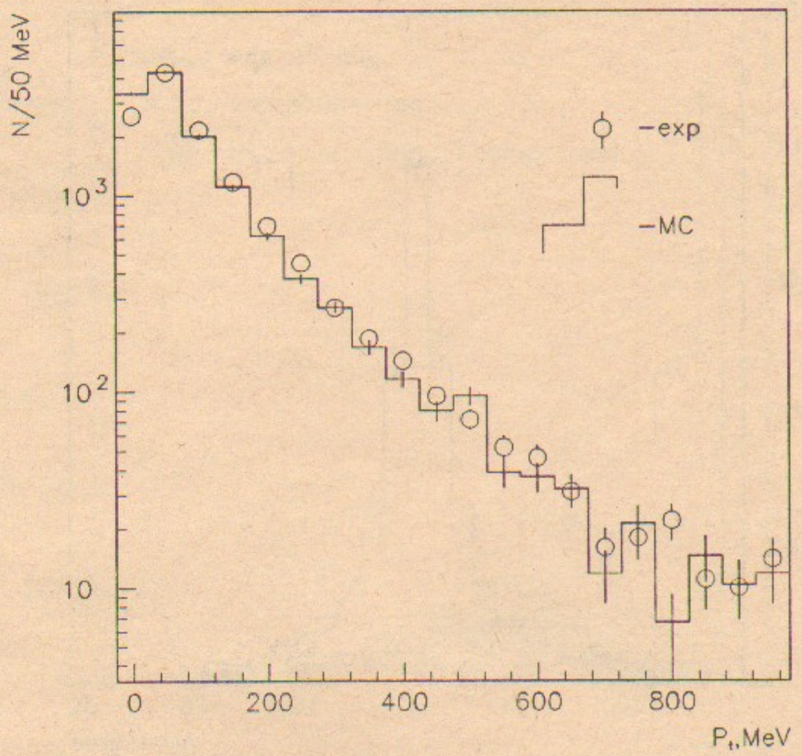

Fig. 10. Transverse momentum distribution for selected pairs.

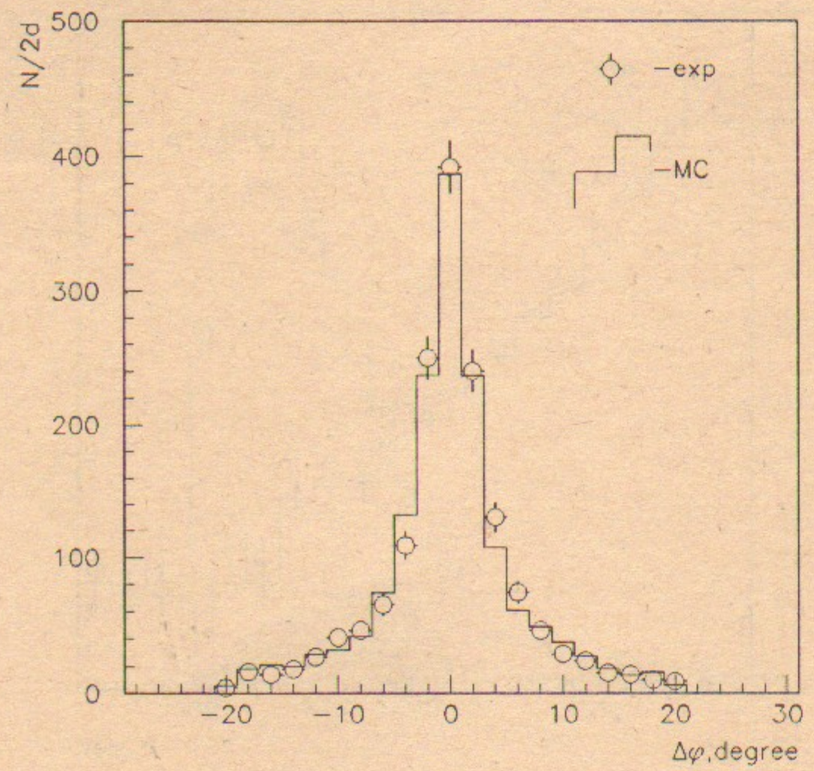

Fig.11. Acomplanarity angle distribution for selected pairs.

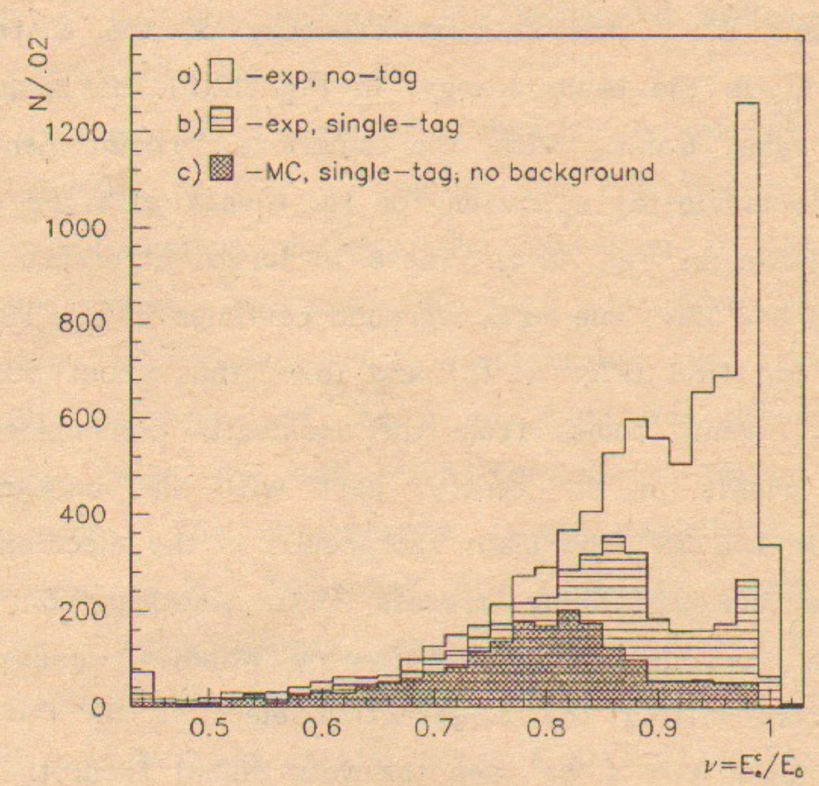

Fig. 12. Calculated energy spectrum of the scattered electrons for selected pairs.

scaled energy $\nu=E_e^c/E_0$ for the selected no-tag events is shown. Here E_e^c is the calculated energy of the scattered electron, E_0 is the beam energy. In Fig. 12(b) the spectrum for the same events with the single-tag requirement is shown. The single-tag spectrum for MC events with the same cuts is shown in Fig. 12(c). There is large difference between 12(b) and 12(c) due to background particles in the TS.

One can find (Fig. 12 (b) and (c)) that about 50% of the tagged events comes from the accidental coincidence of the true events in the central part with the background particles in the TS. The main background is the electrons of the single bremsstrahlung process (SB). Another contribution comes from electromagnetic showers, which are caused by the particles hitting the construction elements of the TS. To reject such events we used the veto signal from the NaI detector, which detects the photons of the SB, and put the restriction for the total number of hits in the proportional chambers of the TS. After applying these cuts the contribution of the background is about 10%. The more detailed examination of the background problem is done below for the determination of the total efficiency of the TS.

The accuracy of the E_e^c calculation is mainly determined by the accuracy of the muon momenta measurement. The resolution $\sigma(\nu)$ is ~1.5% for $\nu=0.8\div1.0$ and increases quickly

for the smaller ν because corresponding muon momenta grow up resulting in σ_p/p increase. The estimated systematic error of E_e^c calculation equals 0.5%.

To check the TS energy calibration we use the parameter $\Delta=(E_e-E_e^c)/E_0$ (Δ^- for e^- and Δ^+ for e^+), where E_e is the measured electron energy. The spectrum of Δ^+ for the selected events is shown in Fig. 13a. The Δ^+ spectrum obtained after background suppression is presented in Fig.13b. The shape of the Δ spectrum was described by a Gaussian with the tail ~$1/\Delta$ for $\Delta<-2\sigma$ taken from MC calculation. The background was described with the polynomial of the 3th order. The free parameters were the number of signal events, peak position, width of signal and all coefficients of polynomial. The number of the signal events are 2451±138 at Fig. 13a and 2108±57 at Fig. 13b. The results on peak positions are $\Delta^+_{peak}=-0.3\pm0.1\%$ and $\Delta^-_{peak}=-1.5\pm0.1\%$. The width (FWHM/2.36) of the spectrum is 3.3±0.10%, which is close to the MC calculation - 3.0±.17%.

The Δ^+ width dependence on the electron energy is shown on Fig. 14. Subtracting the central part contribution one can estimate the TS energy resolution within the region of $\nu=0.7\div1.0$ as $\sigma\ \nu\ =(2.2\pm0.4)\cdot\nu\%$. The MC simulation gives $\sigma\ \nu\ =1.75\cdot\nu\%$ (dashed line in Fig. 14). The results agree within the error to each other and to the result of the

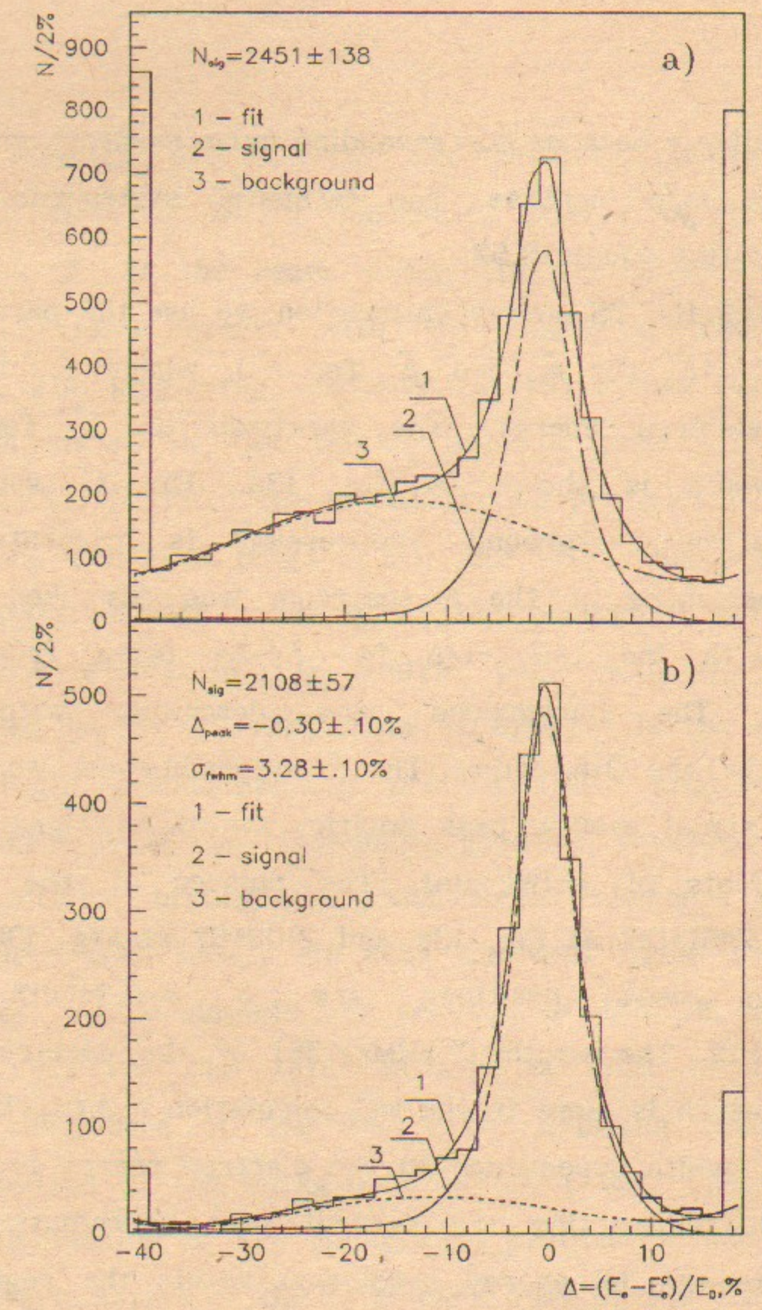

Fig. 13. Spectra on $\Delta^{+}=(E_e-E_e^c)/E_0$ for selected pairs.
a) All events. b) After background suppression.

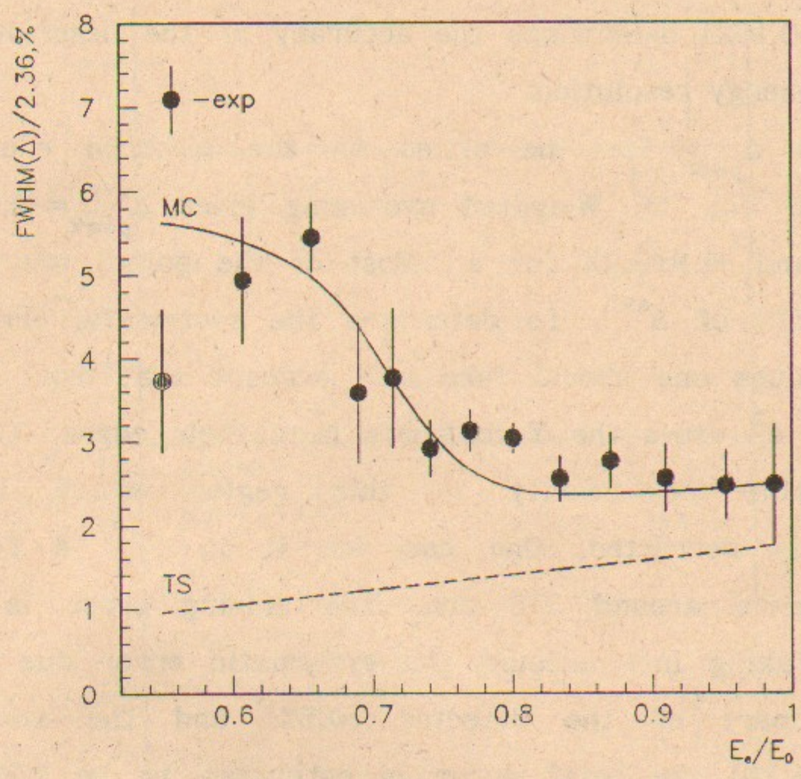

Fig. 14. Dependence of FWHM/2.36 for Δ^{+} on E_e/E_0.

Bhabha scattering - $\sigma(\nu)=(1.70\pm0.10)\%$ for $\nu=1$. The last error (±0.10%) determines the accuracy of the description of the TS energy resolution.

The Δ_{peak} for the slices on the electron energy is shown in Fig. 15. Weighted averaging gives $\Delta^{avr}_{peak}=-0.5\pm0.2\%$ for e^+ and $-1.9\pm0.2\%$ for e^-. Most of the points are placed within ±2% of Δ^{avr}. To determine the systematic errors of these values one should take into account that most of the detected $e^{\pm}$ cross the Y-chambers near their edges. There is considerable nonlinearity in this region which is not completely corrected. One can see it in Fig. 4 for the Y-coordinate around 350 mm. The arising error is about $1\%\cdot E_0$. Taking into account the systematic error due to the central part of the detector (0.5%) and the statistical error (0.2%) the total error is estimated to be 1.2%. The systematic error of the TS energy calibration with the single bremsstrahlung process was 1.5% (section 4). As a result, we conclude that both $\Delta^{\pm}$ agree with zero within a combined error of 1.9%. The time instability for the measured electron energy is less than ±0.5%.

To measure the cross section of $\gamma\gamma$-processes with tagging one should take into account: the position of the chambers with respect to the beam, which determines the dependence of the tagging efficiency ε_t on ν; and the track

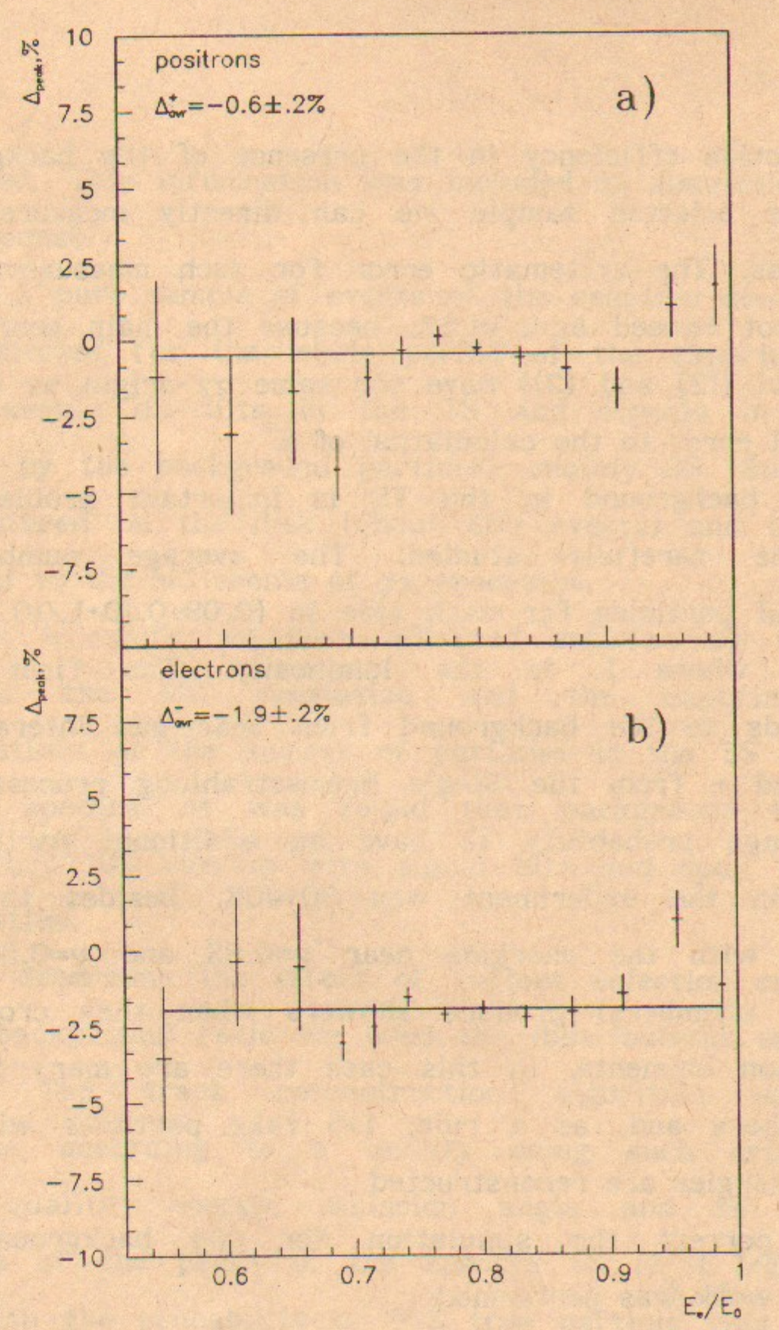

Fig. 15. Dependence of $\Delta^{\pm}_{peak}$ on E_e/E_0.

reconstruction efficiency in the presence of the background. Using the selected sample we can directly measure these efficiencies. The systematic error for such measurement of ε_t will not exceed $\Delta\varepsilon/\varepsilon_t$=1.5%, because the main sources of background ((2) and (3)) have the same $\gamma\gamma$-origin as (1) and give small error to the calculation of E_e^c.

The background in the TS is important problem and should be carefully studied. The average number of background particles for each side is $(0.08+0.10\cdot L/10^{30})$ per collision, where L is the luminosity. The first term corresponds to the background from beam-gas interactions, the second - from the Single Bremsstrahlung process (SB). The average probability to have an additional particle in the TS in the experiment was 30÷40%. Besides that the electrons with the energies near ν=0.85 and ν=0.50 (the edges of chambers) produce showers when they cross the construction elements. In this case there are many hits in the chambers and, as a rule, 1÷5 fake particles with the random energies are reconstructed.

To correct the simulation for the background the following work was performed:

1) Independent measurements of the scattered electron energy (SB in the special runs and selected $\gamma\gamma\rightarrow\mu^+\mu^-$) make possible to understand the conditions when the showers are

produced. This information was included in simulation of the TS response.

2) A pure sample of events of the reaction $ee\rightarrow\mu^+\mu^-$ [12] was selected for the whole period of the experiment. For these events all hits in the TS and signals in NaI are caused by the background particles, mainly SB. Such events were stored on the disk (about 800 events) and then were admixed to the MC events of $\gamma\gamma$-processes.

As a result we have obtained satisfactory agreement between the MC simulation and the experiment for distributions on the number of particles in the TS and their energy spectra. It was found that background hits with probability 10% overlap with signal hits and spoil the track information.

To determine the effect of various selection criteria to signal/background ratio we used the distributions on Δ (Fig. 13a,b). The track reconstruction algorithm sorts the particles according to a quality using such criteria, as track quality, energy, emission angle and so on. The analysis of the peaks in the spectra on $(E_e^c-E_e)/E_0$ shows, that with the probability of 95% true particle gets the best quality. The second and other positions contain about 5% of the true particles with rather small effect/background ratio, therefore only one of all reconstructed particles

was used for the further analysis.

If we use no cuts for the detected electrons the fraction of background particles is 50÷60%, about half of the background is produced by showers. The restriction on the total number of hits (anti-shower cut) decreases the fraction of the showers to 2%. The loss of the "good" electrons is less than 5%, where "good" electron is true particle which measured energy was not spoiled.

The main part of the residual background comes from the SB. Several methods of its suppression were considered. The best way is to measure the energy of the SB photons and reject the electrons satisfying the condition $E_e+E_\gamma=E_0$. However, because of the shield ($3\cdot X_0$ of Pb against the synchrotron radiation) in front of the NaI detector its energy resolution is poor. Additional difficulty is rather high probability to have several photons simultaneously. Due to this reason the NaI detector was used as a threshold device with threshold $E_\gamma=0.15\cdot E_0$.

The other method exploits the fact that the angular distribution for the SB photons $d\vartheta^2/(\vartheta^2+\frac{1}{\gamma}2)^2$ is more narrow than that for the equivalent photons in $\gamma\gamma$-processes $d\vartheta^2/(\vartheta^2+\frac{1}{\gamma}2)$, $\gamma=10^4$. This is also true for the emission angles of the scattered electrons $\vartheta_e=\vartheta_\gamma\cdot\frac{E\gamma}{E_e}$. Rejecting the electrons with $\vartheta_z<5\cdot10^{-4}$ rad (the minimal angle is

determined by the Z-chamber wire spacing) we improve the effect/background ratio.

The modification of spectra on $\Delta^{\pm}$ allows one to perform direct measurements of the efficiency of the selection criteria for the effect events and the background events. The anti-shower cut has the efficiency 95% for the "good" electrons of the effect and ~50% for the background. This cut was used in all further analyses and other efficiencies are calculated after its implying. The first method of single bremsstrahlung suppression (anti-NaI cut) has the efficiency 88% for the effect and 21% for the background. The second method (ϑ_z) gives 61% and 25%. The combination of both - 53% and 11% respectively. The errors of these values don't exceed (2÷3)%. These coefficients are about the same for all $\gamma\gamma$-processes. The effect/background ratio changes from 1 (no cuts at all) to 10 (last case). The first algorithm was used in ref. [7], the second in ref. [30], in ref. [6] the combination of both was required. In our case the first method of background suppression provides the best statistical significance of the signal.

The efficiency of scattered electron tagging ε_t after background suppression (anti-NaI cut) on the electron energy is shown in Fig. 16. Residual backgrounds (about 7%) and true electrons with spoiled energy (about 5%) are also

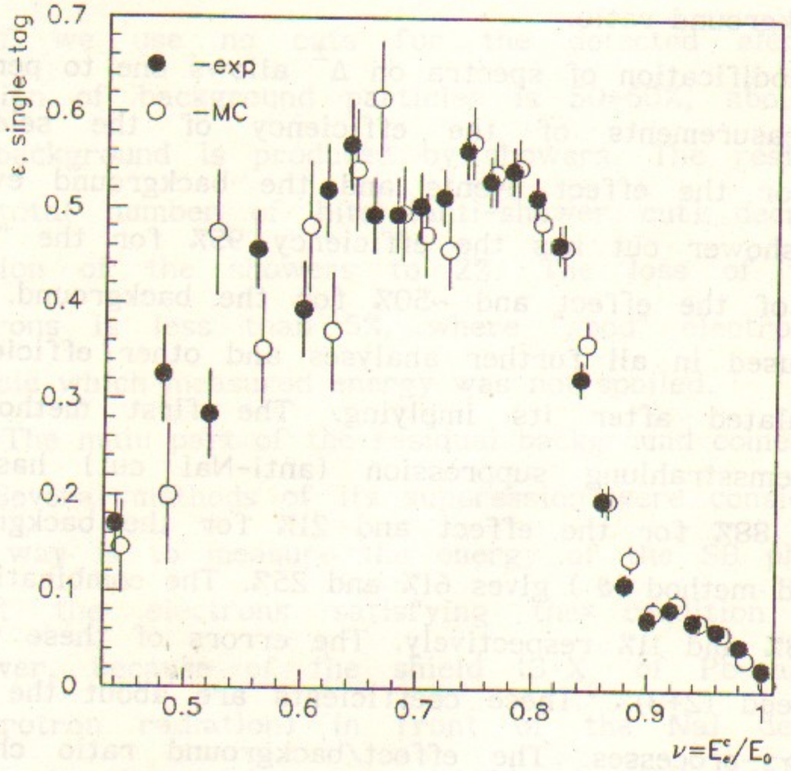

Fig. 16. Efficiency of the scattering electron detection on E_e after background suppression.

contributing to this ε_t. The ratio $\varepsilon_t^{ex}/\varepsilon_t^{MC}$ (where ε^{ex} and ε^{MC} are the tagging efficiencies for experiment and simulation) does not depend on the electron energy and is equal to 0.99±0.03 for e^- and 1.07±0.03 for e^+. The step at $E_{max}=0.84\cdot E_0$ corresponds to the edge of the Y-chamber. Its shift will strongly influence to the total tagging efficiency. The difference between the step position in the experiment and MC is less then $0.7\%\cdot E_0$.

The single-tag efficiency ε_{st} after background suppression as a function of the $M_{inv}(\mu\mu)$ is shown in Fig.17. The ε_{st} is (40÷50)% in the considered mass region, the experiment and the MC agree for all M_{inv} and $\varepsilon_{st}^{ex}/\varepsilon_{st}^{MC}=1.03\pm0.02(stat)\pm0.05(syst)$. The systematic error is connected with the precision of E_{max} and E_{min} ($0.84\cdot E_0$ and $0.51\cdot E_0$) determination and the accuracy of the background simulation.

The most of the selected $\gamma\gamma\to\mu^+\mu^-$ pairs have the invariant mass below 1.5 GeV/c^2. The expected double-tag efficiency for this region is about (2÷3)%. It is rather small because at least one of the detected electrons has to be scattered at relatively large angle. The probability of the accidental coincidence of "true" single-tagged event with the SB in the opposite TS is about 6% and no-tagged event with the SB in the both TS is about 4%. The

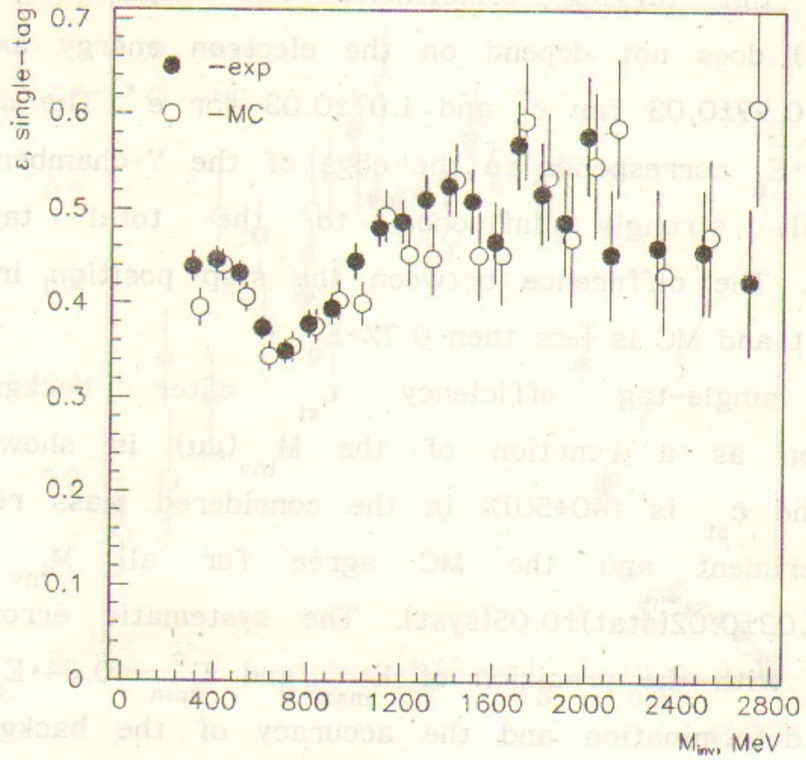

Fig. 17. Single-tag efficiency for the selected pairs on M_{inv} after background suppression.

effect/background ratio for this case is much worse than for the single-tag mode. After the additional cut, ϑ_z>.5 mrad for both scattered electrons, it is possible to see the clear peak in $\Delta M_{\gamma\gamma}$ distribution (Fig. 18), were $\Delta M_{\gamma\gamma}$ is the difference between $M_{inv}(\mu^-\mu^+)$ determined by means of the central part information and the TS information. There are 127±15 events of the signal. The location of the maximum -100±30 MeV is within the expected error of the energy calibration (±100 MeV). The width is 260±30 MeV/c^2. It is determined by the resolution both of the central part and the TS. The width for the MC events is 270±20 MeV/c^2.

After these cuts the double-tag efficiency is 1.4% and the ratio $\varepsilon_{dt}^{ex}/\varepsilon_{dt}^{MC}$=0.90±0.16±0.15. The systematic error is mostly determined by the uncertainty in Y-chamber edge position (E_{max}), because in case of small M_{inv} the most of detected electrons cross the Y-chamber near the edge. This error decreases quickly with growth of M_{inv} above 1.5 GeV/c^2.

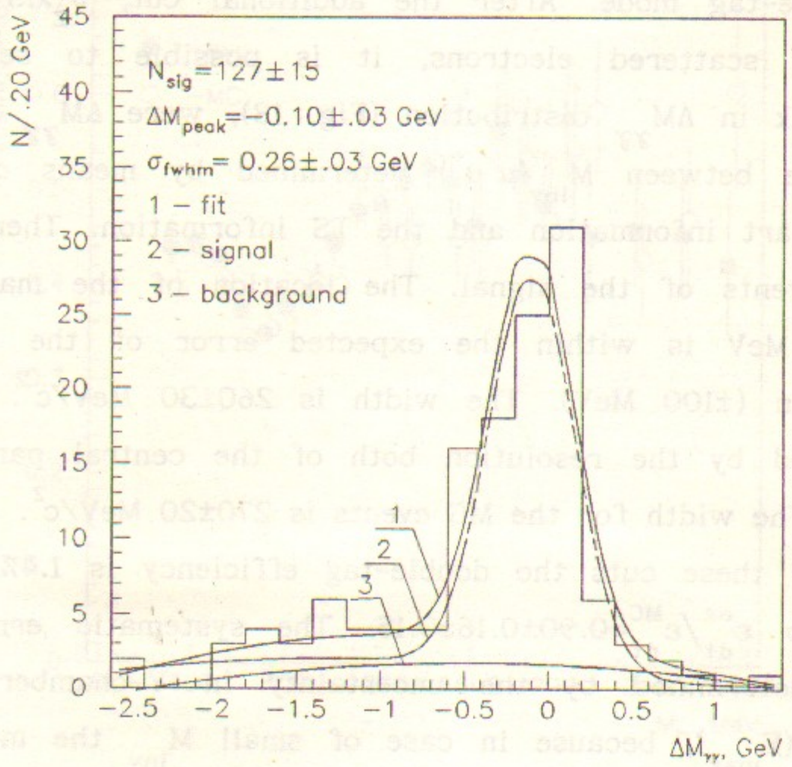

Fig. 18. $\Delta M_{\gamma\gamma}$ spectrum after the "hard" background suppression.

7. Discussion and summary

The main parameters of the TS for studying of the $\gamma\gamma$-processes in single- and double-tag modes are listed below. The most part of them have been obtained with the MC calculation, corrected for backgrounds and inefficiencies. The MC reliability was checked with the selected $\gamma\gamma\rightarrow\mu\mu$ events.

The energy resolution for the tagged electrons $\sigma(E_e)/E_e=(1.75\pm0.1)\%$ is obtained. The systematic error of the electron energy is $\Delta E_e/E_0=1.5\%$. For double-tag mode an invariant mass $M_{\gamma\gamma}$ of the $\gamma\gamma$ system can be measured with the resolution of 200÷110 MeV/c^2 for $M_{\gamma\gamma}$=1÷4 GeV/c^2 (Fig. 19). For the 3 GeV/c^2 resonance (η_c) it corresponds to $\sigma(M_{\gamma\gamma})$=120±10(syst.) MeV/c^2. The systematic error for $M_{\gamma\gamma}$ is about 100 MeV/c^2.

The tagging efficiency ε_t depends on the choice of the background suppression procedure. Some methods were described in section 5. The efficiency values mentioned below are obtained using the anti-shower cut and the veto from the NaI detector (against bremstrahlung). Only particles with unspoiled energies were taken into account.

The single-tag efficiency for the $\gamma\gamma$-events (no selection in central part) is shown in Fig. 20. It is 30÷50% for M_{inv}=0.5÷4.0 GeV/c^2. Some difference between Figs 17 and 20 is connected with the influence of additional cuts in the

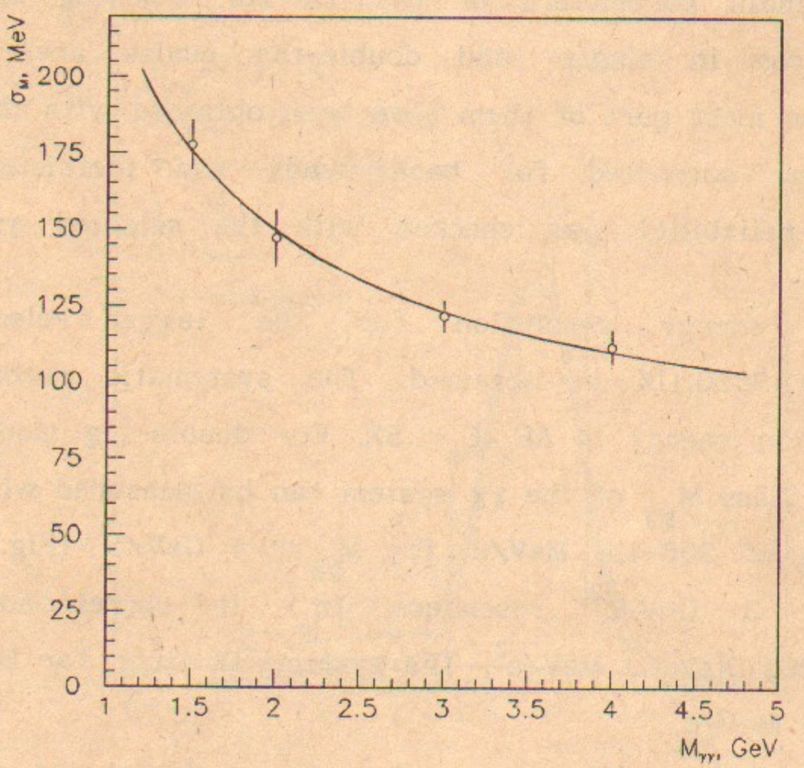

Fig. 19. Dependence of $\sigma(M_{\gamma\gamma})$ on $M_{\gamma\gamma}$ for double-tagged events.

central part used for selection of the $\gamma\gamma\to\mu^+\mu^-$ events and residual backgrounds. The double-tag efficiency is shown in Fig. 21. The maximum efficiency is about 10% for $M_{\gamma\gamma}$=2.5÷3.0 GeV/c^2. For the 3 GeV/c^2 resonance the efficiency is 9.3±0.5(syst.)%. This value is about 2 times less than that for the ideal case when the background is absent. The losses for one detected electron are the following : 3% due to chambers inefficiency, 10% overlapping with background, 5%- anti-shower cut, 5% due to use of only one particle in TS and 12%- anti-NaI cut against bremsstrahlung. This leads to a total inefficiency 30% for single-tagged events and 50% for double-tagged events.

The systematic error of the detection efficiency is determined mainly by the uncertainty in the energy boundaries for detected electrons and the background suppression procedure. The accuracy for E_{min} and E_{max} of the tagged electrons is $\pm 0.7\% \cdot E_0$. It results in the error $\Delta\varepsilon/\varepsilon_{st} \simeq 3\%$ for single-tag mode. For double-tag mode corresponding $\Delta\varepsilon/\varepsilon_{dt}$ varies from 16% to 3% for $M_{\gamma\gamma}$ in the region 1.0÷4.0 GeV/c^2. Other systematic errors come from the background subtraction and chamber inefficiency. The selected events of the process $\gamma\gamma\to\mu\mu$ allowed us to make the direct measurement of the resulting efficiencies. The

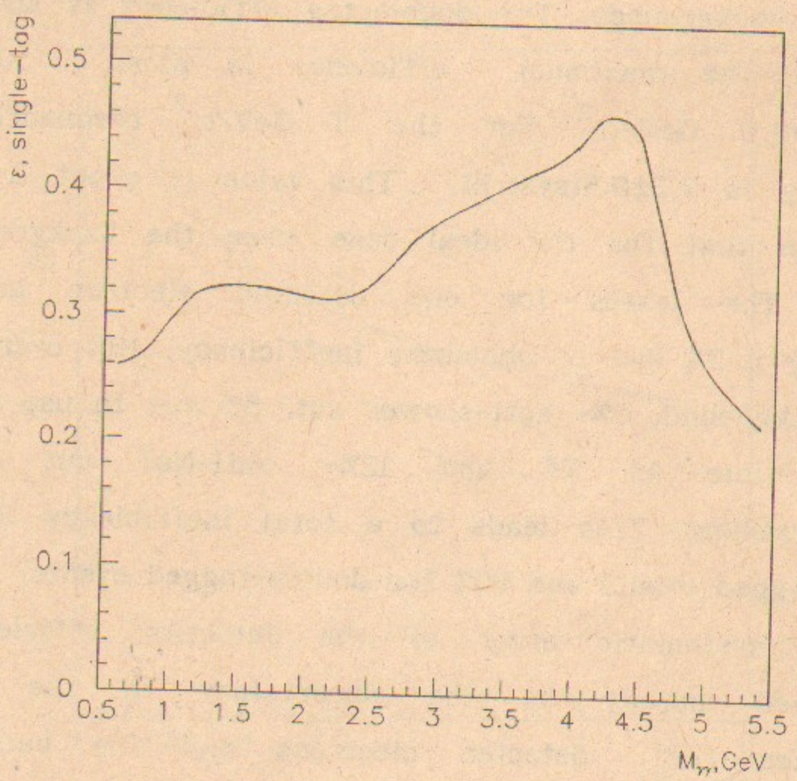

Fig. 20. Single-tag efficiency on $M_{\gamma\gamma}$ after background suppression.

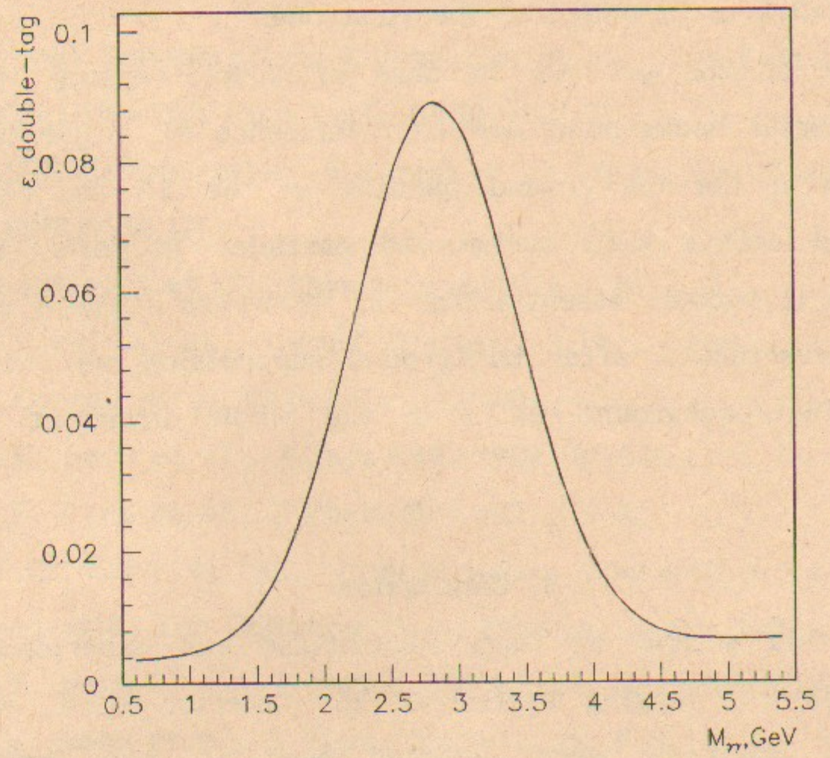

Fig. 21. Double-tag efficiency on $M_{\gamma\gamma}$ after background suppression.

residual systematic error for the tagging efficiency is $\Delta\varepsilon/\varepsilon_t=(2\div3)\%$ to be added to the first one.

One of the problem in case of double-tagging is the combinatorial background due to coincidence of single-tagged events with the background particle in the TS as well as no-tagged events with background particles in both TS. In our case it became essential for $M_{\gamma\gamma}<2$ GeV/c^2, where ε_{dt} is small. Nevertheless after background suppression we obtained good effect/background ratio in the whole invariant mass region.

8. Conclusion

In this article we have summarized our experience of work with the tagging system of the detector MD-1, where scattered electrons were detected even at zero emission angle. The number of results on two-photons physics with single- and double-tagging using this tagging system have been obtained.

This experience was used for designing of the high precision tagging system [31] of the detector KEDR [32], which is under construction in our Institute now.

Acknowledgments

The authors would like to thank the staff of MD-1, VEPP-4 and Computer Center who made this work possible.

REFERENCES

1. TASSO Collaboration, R.Brandelik et al., Phys.Lett. 83B(1979),261; Phys.Lett. 108B(1982),71.
2. JADE Collaboration, W.Bartel et al., Phys. Lett 88B(1979),171.
3. H.J.Bersch et al., Phys.Lett 81(1979), 79.
4. C.Bacci et al., Nuovro Cim.Lett. 3(1979), 709.
5. A.Courau et al.,Phys.Lett 96(1980), 402.
6. S.E. Baru et al., Z.Phys.C48(1990),581-586.
7. S.E. Baru et al., Z.Phys.C53(1992),219-224.
8. S.E. Baru et al., International. Conference on Instrumentation for Colliding Beam Physics, SLAC, 1982.
9. S.E. Baru et al., Preprint INP 83-39, Novosibirsk(1983).
10. S.E. Baru et al., Z.Phys.C30(1986),551-558.
11. A.E. Blinov et al., Nucl. Inst. Meth. A273(1988),31.
12. A.E. Blinov et al., Z.Phys.C48(1992), 229-234.
13. A.E. Bondar et al., Proc. Int. Meeting on Proportional. and Drift Chambers, Dubna(1975),p.219.
14. A.E. Bondar et al., Proc. Int. Meeting on Proportionaland Drift Chambers, Dubna(1978),p.184, V.M. Aulchenko et al.,ibid,p.258.
15. *A.E. Bondar et al., NIM 207(1983), 379.*
16. S.E. Baru et al., Proceeding of the third International.

Conference on Instrumentation for Colliding Beam Physics, Novosibirsk, 1984.

17. V.M. Aulchenko et al., NIM A252(1986), 267-271.
18. A.B.Ivkin et al., Sov.J.Nuc.Phys. 54(1991), 1031.
19. Mark J Collaboration, B.Adeva et al. Phys. Rev. Lett 48(1982),721.
20. PLUTO Collaboration, Ch. Berger et al. Phys. Lett 94B(1980),254.
21. TASSO Collaboration, R. Brandelik et al. Z. Phys. C10(1981),117.
22. Mark II Collaboration, A.Roussarie et al. Phys. Lett 105B(1981),304.
23. PLUTO Collaboration, Ch.Berger et al. Nucl. Phys. B202(1982),189.
24. CELLO Collaboration, H.-J.Behrend et al. Phys. Lett 126(1983),384.
25. A.E. Blinov et al., Z.Phys.C53(1992),33-39.
26. V.M. Budnev et al., Phys.Rep. 15(1975),181.
27. S.E.Brodsky, T.Kinoshita and H.Terazawa, Phys. Rev. D4(1971),1532.
28. F.Berends, P.H.Daverveldt, R.Kleiss, Particle Physics, B253(1985),421.

    F.Berends, P.H.Daverveldt, R.Kleiss, Particle Physics, B253(1985),441.

29. A.D.Bukin et al., Prepr. INP 84-33, Novosibirsk 1984, in Russian.
30. A.E.Blinov et al., Prepr. INP 86-107, Novosibirsk 1986.
31. V.M. Aulchenko et al. 5th International Conference on Instrumentation for colliding beam physics, 1990, p.462.

    V.M. Aulchenko et al., Detector KEDR tagging system for two-photon physics, Preprnt INP 91-49.
32. V.V. Anashin et al., Proceed.of the Int.Symp.on Coordinate detectors, Dubna, 1987